JPET# 244855

Development and translational application of a minimal physiologically-based pharmacokinetic (mPBPK) model for a monoclonal antibody (mAb) against interleukin 23 (IL-23) in IL-23-induced psoriasis-like (PsL) mice

Xi Chen, Xiling Jiang, Rajitha Doddareddy, Brian Geist, Thomas McIntosh, William J Jusko, Honghui Zhou, Weirong Wang

Biologics Development Sciences, Janssen BioTherapeutics, Janssen R&D, 1400 McKean Road, Spring House, PA, 19447, USA (X.C., X.J., R.D., B.G., T.M., W.W.); Department of Pharmaceutical Sciences, School of Pharmacy and Pharmaceutical Sciences, State University of New York at Buffalo, Buffalo, NY, 14214, USA (W.J.J.); Global Clinical Pharmacology, Janssen R&D, Spring House, 1400 McKean Road, Spring House, PA, USA (H.Z.)

X.C., current affiliation: Clinical Pharmacology and Pharmacometrics, Bristol-Myers Squibb, Route 206 & Province Line Road, Princeton, NJ, 08543; X.J., current affiliation: Office of Clinical Pharmacology (OCP), Food and Drug Administration, 10903 New Hampshire Ave, Silver Spring, MD 20993

JPET Fast Forward. Published on February 2, 2018 as DOI: 10.1124/jpet.117.244855
This article has not been copyedited and formatted. The final version may differ from this version.

JPET# 244855

Running Title: A mPBPK model for mAb against IL-23

Corresponding author:

Weirong Wang, Ph.D

Biologics Development Sciences,

Janssen BioTherapeutics, Janssen R&D,

1400 McKean Road, Spring House, Pennsylvania, 19447, USA

Phone: 215-793-7325

Fax: 215-986-1013

e-mail: wwang83@its.jnj.com

Number of text pages: 40

Number of tables: 3

Number of figures: 9

Number of references: 35

Number of words:

Abstract: 192

Introduction: 747

Discussion: 1450

ABBREVIATIONS: IL, interleukin; LLOQ, lower limit of quantification; mAb, monoclonal antibody; mPBPK, minimal physiologically-based pharmacokinetics; PD, pharmacodynamics; PK, pharmacokinetics; Ps, psoriasis; rmIL-23, recombinant mouse IL-23; TMDD, target-mediated drug disposition

Abstract

The IL-23/T_h17/IL-17 immune pathway has been identified to play an important role in the pathogenesis of psoriasis. Many therapeutic proteins targeting IL-23 or IL-17 are currently under development for the treatment of psoriasis. In the present study, a mechanistic PK/PD study was conducted to assess the target-binding and disposition kinetics of a monoclonal antibody (mAb), CNTO 3723, and its soluble target, mouse IL-23, in an IL-23-induced psoriasis-like (PsL) mouse model. A minimal physiologically-based pharmacokinetic (mPBPK) model with target-mediated drug disposition (TMDD) features was developed to quantitatively assess the kinetics and interrelationship between CNTO 3723 and exogenously administered, recombinant mouse IL-23 (rmIL-23) in both serum and lesional skin site. Furthermore, translational applications of the developed model were evaluated with incorporation of human PK for ustekinumab, an anti-human IL-23/IL-12 mAb developed for treatment of psoriasis, and human disease pathophysiology information in psoriatic patients. The results agreed well with the observed clinical data for ustekinumab. Our work provides an example on how mechanism-based PK/PD modeling can be applied during early drug discovery and how preclinical data can be used for human efficacious dose projection and guide decision making during early clinical development of therapeutic proteins.

Introduction

Psoriasis is a chronic immune-mediated inflammatory skin disorder (Schon and Boehncke, 2005). Many cytokines and immune cells have been identified to promote the disease initiation and propagation (Schon and Boehncke, 2005); among those, the IL-23/T_h17/IL-17 immune pathways play pivotal roles (Lima and Kimball, 2010). A recent psoriasis disease model has identified IL-17 secreted by T_h17 cells as one of the key cytokines in psoriasis disease development. T_h17 cells are activated by IL-23 (Nestle et al., 2009; Lowes et al., 2013). In psoriatic patients, both IL-23 and IL-17 exhibit elevated expression in lesional skin sites (Arican et al., 2005). There are several therapeutic mAbs targeting IL-23 and IL-17 for the treatment of psoriasis, including ustekinumab, guselkumab, risankizumab, tildrazumab, secukinumab, and ixekizumab (Hu et al., 2014; Dong and Goldenberg, 2017). These biologics neutralize target cytokines at the lesional skin site, and exert anti-inflammatory activity.

Ustekinumab is an anti-IL-23/IL-12 dual therapeutic monoclonal antibody (mAb) that shows great therapeutic effect for the treatment of psoriasis. It neutralizes both IL-12 and IL-23 by binding to the p40 subunit shared by IL-12 and IL-23. Free cytokine suppression at target tissue sites is anticipated to drive the magnitude and duration of therapeutic effect. Albeit the pharmacokinetics (PK) of ustekinumab in serum have been well-characterized and relationships with pharmacodynamics (PD) has been established with semi-mechanistic PK/PD models (Zhou et al., 2010), less is known about the drug exposure at lesional skin site and its interaction with IL-23 and IL-12 therein. The aim of the present study was to develop mechanistic- and physiologically-based PK/PD models for quantitative characterization of the tissue distribution kinetics of an anti-IL-23 mAb and its IL-23-binding ability in the lesional skin site with a mouse psoriasis-like (PsL) disease model.

Mechanism-based PK/PD models contain quantitative expressions of the causal relationship between drug exposure and pharmacological effects (Danhof et al., 2007). These

components involved in the exposure-response relationship for biologics often include tissue distribution to the target site, target binding and interaction, and downstream pharmacological cascade. More importantly, mechanism-based models distinguish drug- and system-specific characteristics and provide a way to quantitatively translate the PK/PD relationship between preclinical species and humans (Agoram et al., 2007).

The minimal physiologically-based pharmacokinetic (mPBPK) models (Cao and Jusko, 2012; Cao et al., 2013) inherit and lump major physiologic attributes from the whole-body PBPK models and generate physiologically-relevant PK parameters, while allowing for assessment of any tissue of interest with the flexibility to add additional tissue compartments. Importantly, with measurements of target interaction in blood or specific tissues of interest, the mPBPK model can incorporate dynamics of target binding and disposition by implementing target-mediated drug disposition (TMDD) kinetics into plasma or the specific tissue compartments (Cao and Jusko, 2014). The first-generation mPBPK model (Cao and Jusko, 2012) is more applicable to small molecule drugs or small size proteins. The model includes blood/plasma and one or more lumped tissue compartments. Drug tissue distribution is assumed to be driven by the Fick's Law of diffusion. The second-generation mPBPK model is more suitable for biologics such as mAbs (Cao et al., 2013). It adapts all essential components of the full PBPK models for biologics. Tissues are lumped into two compartments (tight or leaky) based on their vascular endothelial structure. Para-vascular convection and lymph drainage are assumed to be the dominant pathways for biologics uptake and removal from tissues (Cao et al., 2013).

Our group has previously published work on applying the mPBPK modeling approach to quantitatively assess the kinetics and interrelationship between an anti-IL-6 mAb and IL-6 in both serum and joint lavage fluid in a mouse collagen-induced arthritis (CIA) model (Chen et al., 2016). A second example focusing on the interplay between an anti-IL-23 mAb and IL-23 in both serum and lesional skin site is presented here.

Repeated intradermal (ID) injection of recombinant murine (rm)IL-23 into the ear of a mouse induces psoriasis-like (PsL) epidermal hyperplasia, which serves as a suitable preclinical disease model for investigating drug candidates targeting the IL-23/T_h17/IL-17 pathway for psoriatic indications (Kopp et al., 2003; Chan et al., 2006; Rizzo et al., 2011). A mechanistic study was conducted to assess the binding and disposition kinetics of CNTO 3723, a mAb, and its target rmIL-23 in this model. A mPBPK model incorporating TMDD was developed to quantitatively assess the kinetics and interrelationship between CNTO 3723 and rmIL-23 in both serum and lesional skin site. Potential application of this model in translational pharmacology was examined by comparing model predictions to observed ustekinumab effect in psoriatic patients.

Methods

Test Articles

A rat anti-mouse IL-23 mAb, CNTO 3723, was produced at Janssen R&D, LLC (Spring House, PA, USA) and used in the study. Recombinant murine IL-23 (rmIL-23) was purchased from eBioscience (San Diego, CA, USA, cat# 14-8231-63) and used for development of IL-23-induced PsL mouse disease model.

Animal Study Design and Sample Collection

The in-life part of the animal study was conducted at WuXi AppTec (Suzhou, China). All studies were approved by the Institutional Animal Care and Use Committee (IACUC) of WuXi AppTec.

CNTO 3723 and rmIL-23 PK characterization

Healthy C57BL/6 WT female mice (n = 52) were randomly assigned to 3 groups (Groups A – C) to study the PK of CNTO 3723 and rmIL-23. Animals in Group A (n = 12) received a single IV bolus dose of CNTO 3723 at 10 mg/kg. Animals in Group B (n = 16) received a single

IV bolus dose of rmIL-23 at 400 ng. Animals in Group C (n = 24) received a single intra-dermal (ID) dose of rmIL-23 at 400 ng into the left ear. Terminal and retro-orbital blood samples were collected at various sampling time points (**Table 1**).

Target engagement (TE) assessment in IL-23-induced PsL mouse model

Our previous data had shown that daily ID injection of rmIL-23 for five consecutive days can induce psoriasis-like inflammation as reflected by ear thickness, ear weight and histopathology analysis (N. Rozenkrants, internal data).

A second set of C57BL/6 WT female mice (n = 45 × 4) were randomly assigned to 4 groups (Groups D – G) to study CNTO 3723 target engagement in IL-23-induced PsL mouse disease model. Animals in Groups D, E, F and G received a single IV bolus dose of CNTO 3723 at 3.3, 3.3, 10 and 3.3 mg/kg on Study Day 0, respectively, and five consecutive daily ID injection of rmIL-23 at 50, 200, 200 and 500 ng, respectively, in 10 µL of PBS/ 0.1% bovine serum albumin (BSA) on Study Days 2, 3, 4, 5 and 6, respectively, into the lateral left ear. Another 20 mice in Group H were administrated with an IV bolus dose of CNTO 3723 at 10 mg/kg on Study Day 0 and an ID injection of 200 ng rmIL-23 into left ear on Study Day 2. Terminal and retro-orbital blood samples were collected at various sampling time points (**Table 1**). At all terminal sampling time points, an 8 mm biopsy punch of each of the two ears were collected from the animal, and tissue homogenate was prepared with Qiagen TissueLyser II (30 Hz x 2 min) in 500 µL of homogenization buffer containing 1xPBS with 0.1% BSA, 1% Triton X-100 and 2% (v/v) Protease Inhibitors. The homogenate was centrifuged at 12000× g for 15 min at 4ºC and the collected supernatants was stored at -80°C until analysis.

Bioanalytical Methods

The concentration of CNTO 3723 in serum and ear tissue homogenates were quantified by a fluorescence-based immunoassay on the Gyrolab™xP platform (Gyros AB, Uppsala, Sweden). The lower limits of quantification (LLOQ) for serum and ear tissue homogenates

JPET Fast Forward. Published on February 2, 2018 as DOI: 10.1124/jpet.117.244855
This article has not been copyedited and formatted. The final version may differ from this version.

CNTO 3723 concentrations were both 80 ng/mL. The concentration of total and free rmIL-23 concentrations in serum and ear tissue homogenate were determined using an electrochemiluminescence-based immunoassay (ECLIA) using the Meso Scale Discovery (MSD®) platform (Meso Scale Discovery, Rockville, MD, USA) with LLOQ of 27.4 pg/mL for both total and free rmIL-23 concentration in serum and 9.14 pg/mL for both total and free rmIL-23 concentration in ear tissue homogenates.

A mPBPK Model to Characterize the Interplay between CNTO 3723 and rmIL-23 in IL-23-induced PsL Mice

The mPBPK model with TMDD features was adapted to characterize the interrelationship between CNTO 3723 and rmIL-23 in IL-23-induced PsL mice. The pharmacokinetics of CNTO 3723 and rmIL-23 in mice were first characterized using a second-generation and a first-generation mPBPK models (Step I and II), respectively. Alteration of CNTO 3723 and rmIL-23 pharmacokinetics due to repeated ID injections of rmIL-23 into mouse ear were subsequently assessed (Step III). At last, the mPBPK models for rmIL-23 and CNTO 3723 were overlaid with TMDD features incorporated to characterize the interrelationship between CNTO 3723 and rmIL-23 (Step IV).

Step I: Serum pharmacokinetics of CNTO 3723

Serum concentration profiles of CNTO 3723 in animal Group A were described with the second-generation mPBPK model. The model includes serum, lymph, and two lumped tissue compartments (leaky and tight, based on vascular endothelium structures) connected in an anatomical manner (**Figure 1a**). The model was described as:

$$\frac{dC_s}{dt} = \frac{C_{lymph} \cdot L - C_s \cdot L_1 \cdot (1-\sigma_1) - C_s \cdot L_2 \cdot (1-\sigma_2) - C_s \cdot CL_s}{V_s} \qquad \mathrm{C_s}(0) = \frac{\mathrm{Dose}}{\mathrm{V_s}} \quad (1)$$

JPET Fast Forward. Published on February 2, 2018 as DOI: 10.1124/jpet.117.244855
This article has not been copyedited and formatted. The final version may differ from this version.

$$\frac{dC_{tight}}{dt} = \frac{C_s \cdot L_1 \cdot (1-\sigma_1) - L_1 \cdot (1-\sigma_L) \cdot C_{tight}}{V_{tight}} \qquad C_{tight}(0) = 0 \quad (2)$$

$$\frac{dC_{leaky}}{dt} = \frac{C_s \cdot L_2 \cdot (1-\sigma_2) - L_2 \cdot (1-\sigma_L) \cdot C_{leaky}}{V_{leaky}} \qquad C_{leaky}(0) = 0 \quad (3)$$

$$\frac{dC_{lymph}}{dt} = \frac{L_1 \cdot (1-\sigma_L) \cdot C_{tight} + L_2 \cdot (1-\sigma_L) \cdot C_{leaky} - C_{lymph} \cdot L}{V_{lymph}} \qquad C_{lymph}(0) = 0 \quad (4)$$

where C_s, C_{tight} and C_{leaky} are concentrations of CNTO 3723 in serum and interstitial fluid (*ISF*) in two types of lumped tissues categorized by continuous and fenestrated vascular endothelium, and C_{lymph} is the concentration of CNTO 3723 in lymph. The V_{tight} (0.65 • *ISF* • K_p, where K_p is the available fraction of *ISF* for antibody distribution) and V_{leaky} (0.35 • *ISF* • K_p) are *ISF* volumes of the two lumped tissues (Cao et al., 2013). The V_{lymph} represents lymph volume, which is assumed equal to blood volume. The L is total lymph flow rate and L_1 and L_2 account for 1/3 and 2/3 of the total lymph flow (Cao et al., 2013). The σ_1 and σ_2 are vascular reflection coefficients for leaky and tight tissues. The σ_L is the lymphatic capillary reflection coefficients and is assumed to be 0.2 (Cao et al., 2013). CL_s represents the linear serum clearance of CNTO 3723.

Step II: Pharmacokinetics of rmIL-23

The serum and ear homogenates concentration profiles of rmIL-23 in animal Groups B and C were fitted with a first-generation mPBPK model to characterize the pharmacokinetics of rmIL-23. The model has a serum compartment and lumps all tissues into one tissue compartment (**Figure 1b**). Following IV bolus administration, the model is described as:

$$\frac{dC_{s\,IL23}}{dt} = \frac{-C_{s\,IL23} \cdot (CL_{s\,IL23} + f_d \cdot Q_{CO}) + \frac{C_{t\,IL23}}{K_p} \cdot f_d \cdot Q_{CO}}{V_s} \qquad C_{s\,IL23}(0) = \frac{Dose}{V_s} \quad (5)$$

$$\frac{dC_{t\,IL23}}{dt} = \frac{C_{s\,IL23} \cdot f_d \cdot Q_{CO} - \frac{C_{t\,IL23}}{K_p} \cdot f_d \cdot Q_{CO}}{V_t} \qquad C_{tIL23}(0) = 0 \quad (6)$$

JPET Fast Forward. Published on February 2, 2018 as DOI: 10.1124/jpet.117.244855
This article has not been copyedited and formatted. The final version may differ from this version.

where $C_{s\ IL23}$ and $C_{t\ IL23}$ are concentrations of rmIL-23 in serum (V_s) and tissue *ISF* (V_t), Q_{CO} is the cardiac plasma flow (Cao and Jusko, 2012), f_d is the fraction of Q_{CO} for V_t, K_p is the tissue partition coefficient and CL_{sIL23} is the serum clearance.

The absorption kinetics following ID injection of rmIL-23 in the ear was assumed to be mixed exponential-decay and constant first-order absorption kinetics. Following ID injection in the ear, the model is described as:

$$\frac{dA_{ear\ IL23}}{dt} = -\left(k_{inj} \cdot e^{-k_{dim} \cdot t} + k_{abs}\right) \cdot A_{ear} \qquad A_{ear}(0) = Dose \qquad (7)$$

$$\frac{dC_{s\ IL23}}{dt} = \frac{\left(k_{inj} \cdot e^{-k_{dim} \cdot t} + k_{abs}\right) \cdot F \cdot A_{ear\ IL-23} - C_{s\ IL23} \cdot (CL_{s\ IL23} + f_d \cdot Q_{CO}) + \frac{C_{t\ IL23}}{K_p} \cdot f_d \cdot Q_{CO}}{V_s}$$

$$C_{s\ IL23}(0) = 0 \qquad (8)$$

$$\frac{dC_{t\ IL23}}{dt} = \frac{C_{s\ IL23} \cdot f_d \cdot Q_{CO} - \frac{C_{t\ IL23}}{K_p} \cdot f_d \cdot Q_{CO}}{V_t} \qquad C_{t\ IL23}(0) = 0 \qquad (9)$$

where A_{ear} is the amount of rmIL-23 at the site of injection, k_{inj} is the first-order absorption rate constant caused by blister formation following ID injection and k_{dim} is the exponential decay factor to describe blister healing process, k_{abs} is the first-order absorption rate constants from dermis, F presents the bioavailability. The remaining symbols are the same as previously defined.

The measured concentration of rmIL-23 in ear homogenates is described as:

$$C_{ear\ IL23} = \frac{A_{ear\ IL23}}{V_{buffer}} \times \alpha_{rec} \qquad (10)$$

where V_{buffer} is the volume of buffer used to prepare ear tissue homogenate (V_{buffer} = 0.5 mL) and α_{rec} is the recovery rate of rmIL-23 following tissue sampling and homogenate procedures (α_{rec} = 10%).

JPET Fast Forward. Published on February 2, 2018 as DOI: 10.1124/jpet.117.244855
This article has not been copyedited and formatted. The final version may differ from this version.

Step III: Impact of repeated ID injection of rmIL-23 on the pharmacokinetics of rmIL-23 and CNTO 3723

Our data showed that repeated ID injections of rmIL-23 in mouse ear led to alteration in the pharmacokinetics for both rmIL-23 and CNTO 3723 (See **Figure 3** for details).

Impact on rmIL-23 absorption

Following repeated rmIL-23 administration, the apparent decrease in the rate of absorption of rmIL-23 from ear following each additional dose was described by a decrease of the first-order absorption rate constant (k_{abs}). The concentration profiles of total rmIL-23 in ear homogenates in Groups D – H were applied to fit with the absorption kinetics model (Equation 7). Parameters related to rmIL-23 ID absorption estimated previously ('Step II: Pharmacokinetics of rmIL-23') were fixed. To account for the alteration in rmIL-23 absorption kinetics, k_{abs} following the nth dose is described as:

$$k_{abs\_N} = k_{abs} \cdot \left(1 - (N_{ID} - 1) \cdot fac_{lym}\right) \quad (10)$$

where N_{ID} represents the n^{th} rmIL-23 ID injection and fac_{lym} is the ratio decrease in k_{abs} following each rmIL-23 ID dose. The remaining symbols are the same as previously defined.

Impact on CNTO 3723 disposition

Upon ID injection of rmIL-23 into mouse ear, the CNTO 3723 concentration profiles in ear homogenates exhibited an apparently enhanced and oscillated tissue distribution. The distribution kinetics of CNTO 3723 in mouse ear skin were characterized by incorporating an 'ear skin' compartment into the second-generation mPBPK model (**Figure 1c**). CNTO 3723 concentration profiles in serum and ear homogenates in healthy control and IL-23-induced PsL mice (Groups A and D – H) were examined. Parameters related to CNTO 3723 serum pharmacokinetics estimated previously ('Step I: Pharmacokinetics of CNTO 3723') were fixed. Together with Equations 1 – 5, the model addition is:

JPET Fast Forward. Published on February 2, 2018 as DOI: 10.1124/jpet.117.244855
This article has not been copyedited and formatted. The final version may differ from this version.

$$\frac{dC_{ear\ ISF}}{dt} = \frac{C_s \cdot V_{ear\ ISF} \cdot k_{ear} \cdot (1-\sigma_{ear}) - C_{ear\ ISF} \cdot V_{ear\ ISF} \cdot k_{ear} \cdot \left(1 - scal \cdot e^{-d_{lym} \cdot T_{postIL23}}\right) \cdot (1-\sigma_L)}{V_{ear\ ISF}}$$

$$C_{ear\ ISF}(0) = 0 \qquad (11)$$

where $C_{ear\ ISF}$ represents CNTO 3723 concentration in mouse ear *ISF* space ($V_{ear\ ISF}$), k_{ear} is the ear *ISF* turnover rate and represented as lymph flow rate (L_{ear}) divided by $V_{ear\ ISF}$, the σ_{ear} is the vascular reflection coefficient for mouse ear skin. The remaining symbols are the same as previously defined. The quantity of CNTO 3723 in mouse ear biopsy puncture is minimal comparing to that in systemic circulation. Therefore, the impact of CNTO 3723 outflow from mouse ear on serum CNTO 3723 was not included.

For healthy control mice before rmIL-23 injection:

$$\sigma_{ear} = \sigma_{ear\ ctrl} \qquad (12a)$$

For IL-23-induced PsL mice (mice after rmIL-23 injection on day 2):

$$\sigma_{ear} = \sigma_{ear\ PsL} \qquad (12b)$$

Immediately following each rmIL-23 treatment, the CNTO 3723 concentration in ear homogenates exhibited a transient increase and then decreased as CNTO 3723 gets eliminated from serum (**Figure 3a**). The term ($1 - scal \cdot e^{-d_{lym} \cdot T_{postIL23}}$) is applied to account for the oscillation of CNTO 3723 concentration profiles in ear homogenates following ID injection of rmIL-23, where *scal* is the maximum decrease in the ear skin lymph flow rate immediately following each rmIL-23 ID injection, d_{lym} is the exponential rate constant of remission of lymph propulsion, and $T_{postIL23}$ represents the time post rmIL-23 administration.

The measured concentration of CNTO 3723 in ear homogenates is described as:

$$C_{ear} = \frac{C_{ear\ ISF} \cdot V_{ear\ ISF} + C_s \cdot V_{ear\ Vas}}{V_{buffer}} \qquad (13)$$

where $V_{ear\ ISF}$ and $V_{ear\ Vas}$ are the volume of *ISF* and residual vascular space of ear skin biopsy sample (W_{ear}). For mice in healthy control group (Group A) and mice in rmIL-23 treatment

JPET Fast Forward. Published on February 2, 2018 as DOI: 10.1124/jpet.117.244855
This article has not been copyedited and formatted. The final version may differ from this version.

groups (Groups D – H) prior day 2, W_{ear} was on average of 10 mg. Upon rmIL-23 administration post day 2 in Groups D – H, ear weight and thickness increased, the W_{ear} was on average of 15 mg. *ISF* and residual vascular spaces account for 15% and 5% of the total tissue volume, assuming 1 g equals to 1 mL. The remaining symbols are the same as previously defined.

Step IV: Interrelationship between CNTO 3723 and rmIL-23

The interrelationship between CNTO 3723 and rmIL-23 was assessed by overlaying the first- and second-generation mPBPK models with TMDD features incorporated (**Figure 1d**). CNTO 3723, and free and total rmIL-23 concentration profiles in serum and ear homogenates in Groups D – H were applied to simultaneously fit with the model. Free rmIL-23 concentrations in serum were below LLOQ at all the time points and were not used for model development. Parameters that have been estimated from previous steps were fixed. The model assumed rmIL-23 and CNTO 3723 binding in ear tissue homogenates reached equilibrium and had the binding dissociation constant (K_D) estimated. The model is described as:

$$\frac{dC_s}{dt} = \frac{C_{lymph} \cdot L - C_{free} \cdot L_1 \cdot (1-\sigma_1) - C_{free} \cdot L_2 \cdot (1-\sigma_2) - C_{free} \cdot CL_s}{V_s} - AR \cdot k_{int}$$

$$C_s(0) = \frac{Dose}{V_p} \quad (14)$$

$$\frac{dC_{tight}}{dt} = \frac{C_{free} \cdot L_1 \cdot (1-\sigma_1) - L_1 \cdot (1-\sigma_L) \cdot C_{tight}}{V_{tight}} \qquad C_{tight}(0) = 0 \quad (15)$$

$$\frac{dC_{leaky}}{dt} = \frac{C_{free} \cdot L_2 \cdot (1-\sigma_2) - L_2 \cdot (1-\sigma_L) \cdot C_{leaky}}{V_{leaky}} \qquad C_{leaky}(0) = 0 \quad (16)$$

$$\frac{dC_{lymph}}{dt} = \frac{L_1 \cdot (1-\sigma_L) \cdot C_{tight} + L_2 \cdot (1-\sigma_L) \cdot C_{leaky} - C_{lymph} \cdot L}{V_{lymph}} \qquad C_{lymph}(0) = 0 \quad (17)$$

$$\frac{dC_{ear\ ISF}}{dt} =$$

$$\frac{C_{free} \cdot V_{ear\ ISF} \cdot k_{ear} \cdot (1-\sigma_{ear}) - C_{ear\ ISF} \cdot V_{ear\ ISF} \cdot k_{ear} \cdot \left(1 - scal \cdot e^{-d_{lym} \cdot T_{postIL23}}\right) \cdot (1-\sigma_L)}{V_{ear\ ISF}}$$

JPET Fast Forward. Published on February 2, 2018 as DOI: 10.1124/jpet.117.244855
This article has not been copyedited and formatted. The final version may differ from this version.

$$C_{ear\ ISF}(0) = 0 \qquad (18)$$

$$\frac{dA_{ear\ IL23}}{dt} = -\left(k_{inj} \cdot e^{-k_{dim} \cdot t} + k_{abs}\right) \cdot A_{ear\ IL23} \qquad A_{ear}(0) = Dose \qquad (19)$$

$$\frac{dC_{s\ IL23}}{dt} =$$

$$\frac{\left(k_{inj} \cdot e^{-k_{dim} \cdot t} + k_{abs}\right) \cdot F \cdot A_{ear\ IL23} \cdot 0.05 - (C_{s\ IL23} - AR) \cdot CL_{sIL23} - C_{s\ IL23} \cdot f_d \cdot Q_{CO} + \frac{C_{t\ IL23}}{K_p} \cdot f_d \cdot Q_{CO}}{V_s}$$

$$- AR \cdot k_{int} \qquad C_{s\ IL23}(0) = 0 \qquad (20)$$

$$\frac{dC_{t\ IL23}}{dt} = \frac{C_{s\ IL23} \cdot f_d \cdot Q_{CO} - \frac{C_{t\ IL23}}{K_p} \cdot f_d \cdot Q_{CO}}{V_t} \qquad C_{t\ IL23}(0) = 0 \qquad (21)$$

where C_{free} is the free CNTO 3723 concentration in serum, C_{sIL23} is the total rmIL-23 concentration in serum, and *AR* is the CNTO 3723-rmIL-23 complex concentration in serum, k_{int} is the elimination rate constant of the CNTO 3723-rmIL-23 complex in serum. The remaining symbols are the same as previously described. In addition, in Equation 20, an arbitrary factor of 0.05 was applied to adjust the absorption of rmIL-23 in serum from ID injection in ear based on the observed serum level of rmIL-23.

Assuming quasi-equilibrium condition, the free CNTO 3723 concentration in serum (C_{free}) can be described as (Gibiansky et al., 2008):

$$C_{free} = \frac{(C_s - K_{ss} - C_{sIL23}) - \sqrt{(C_s - K_{ss} - C_{sIL23})^2 + 4 \cdot C_s \cdot K_{ss}}}{2} \qquad (22)$$

The K_{ss} is the steady-state constant defined as:

$$K_{ss} = \frac{k_{int} + k_{off}}{k_{on}} \qquad (23)$$

where the k_{on} and k_{off} refer to the CNTO 3723-IL-23 association and dissociation rate constants. *AR* can be described as:

$$AR = C_{sIL23} \cdot \frac{C_{free}}{K_{ss} + C_{free}} \qquad (24)$$

JPET Fast Forward. Published on February 2, 2018 as DOI: 10.1124/jpet.117.244855
This article has not been copyedited and formatted. The final version may differ from this version.

Assuming rmIL-23 and CNTO 3723 in ear tissue homogenates reached binding equilibrium, the free concentration of CNTO 3723 in ear homogenate ($C_{free\ EH}$) was described as (Gibiansky et al., 2008):

$$C_{free\ EH} = \frac{(C_{ear} - K_D - C_{ear\ IL23}) - \sqrt{(C_{ear} - K_D - C_{ear\ IL23})^2 + 4 \cdot C_{ear} \cdot K_D}}{2} \quad (25)$$

where C_{ear} and $C_{ear\ IL23}$ are the measured concentrations of total CNTO 3723 and rmIL-23 in ear tissue homogenates previously defined in Equations 13 and 10. K_D is the binding dissociation coefficient (k_{off} / k_{on}).

The free rmIL-23 concentration in ear homogenates is:

$$C_{ear\ fIL23} = C_{ear\ IL23} \cdot \frac{K_D}{K_D + C_{free\ EH}} \quad (26)$$

Prediction of Ustekinumab Effect in Humans

To evaluate the translational utility of the developed preclinical mechanism-based mPBPK model, the mPBPK model results, ustekinumab human PK and psoriatic patient disease pathophysiology information were integrated to predict ustekinumab effect in psoriatic patients. The integrated information included: 1) CNTO 3723 tissue distribution kinetics and interaction with rmIL-23 in serum and lesional skin sites in IL-23-induced PsL mice, and these parameters were assumed to be the same in psoriatic patients 2) serum ustekinumab pharmacokinetics in psoriatic patients (Zhu et al., 2010), 3) ustekinumab binding affinity with human IL-23 (internal data), and 4) IL-23 baseline concentrations in healthy and psoriatic patients (El Hadidi H, 2008). The model structure for translational PK/PD application was shown in **Figure 2**. Model includes only the central compartment and the lesional skin compartment. Serum concentration of ustekinumab in psoriatic patients was used as the driving function for its distribution and exposure in lesional skin sites (dashed lines and arrows). The tissue distribution kinetics is governed by lymph flow turnover rate of skin (k_{skin}) and vascular permeability (σ_{skin}). TMDD

JPET Fast Forward. Published on February 2, 2018 as DOI: 10.1124/jpet.117.244855
This article has not been copyedited and formatted. The final version may differ from this version.

features were incorporated in both serum and lesional skin compartments for characterization of the interaction of ustekinumab with IL-23. The model was described as:

$$\frac{dC_{s\,mAb}}{dt} = \frac{input - C_{s\,fmAb} \cdot CL - k_{s\,int} \cdot AR_s \cdot V}{V} \qquad C_{s\,mAb}(0) = 0 \quad (27)$$

$$\frac{dC_{t\,mAb}}{dt} = C_{s\,fmAb} \cdot k_{skin} \cdot (1 - \sigma_{skin}) - C_{t\,fmAb} \cdot k_{skin} \cdot (1 - \sigma_L) - AR_t \cdot k_{t\,int}$$

$$C_{t\,mAb}(0) = 0 \quad (28)$$

$$\frac{dC_{s\,IL23}}{dt} = k_{s\,syn} - k_{s\,deg} \cdot (C_{s\,IL23} - AR_s) - AR_s \cdot k_{s\,int} \qquad C_{s\,IL23}(0) = C_{s\,IL23b} \quad (29)$$

$$\frac{dC_{t\,IL23}}{dt} = k_{t\,syn} - k_{t\,deg} \cdot (C_{t\,IL23} - AR_t) - AR_t \cdot k_{t\,int} \qquad C_{s\,IL23}(0) = C_{t\,IL23b} \quad (30)$$

where $C_{s\,mAb}$, $C_{t\,mAb}$, $C_{s\,IL23}$ and $C_{t\,IL23}$ are total concentrations of ustekinumab and IL-23 concentration in serum and lesional skin *ISF*. $C_{s\,fmAb}$ an $C_{t\,fmAb}$ are free ustekinumab concentrations in serum and lesional skin *ISF*. AR_s and AR_t are the ustekinumab-IL-23 complex concentrations in serum and lesional skin *ISF*. *CL* and *V* are the clearance and volume of ustekinumab of the central compartment. $k_{s\,int}$ and $k_{t\,int}$ are the serum and skin tissue elimination rate constants of AR_s and AR_t. $k_{s\,syn}$, $k_{s\,deg}$, $k_{t\,syn}$ and $k_{t\,deg}$ are the synthesis and degradation rate constants of IL-23 in serum and skin *ISF*. $C_{s\,IL23b}$ and $C_{t\,IL23b}$ represent the baseline concentrations of IL-23 in psoriatic patients.

Assuming quasi-equilibrium condition, $C_{s\,fmAb}$ an $C_{t\,fmAb}$ can each be described as (Gibiansky et al., 2008):

$$C_{s\,fmAb} = \frac{(C_{s\,mAb} - K_{s\,ss} - C_{s\,IL23}) - \sqrt{(C_{s\,mAb} - K_{s\,ss} - C_{s\,IL23})^2 + 4 \cdot C_{s\,mAb} \cdot K_{s\,ss}}}{2} \quad (31)$$

$$C_{t\,fmAb} = \frac{(C_{t\,mAb} - K_{t\,ss} - C_{t\,IL23}) - \sqrt{(C_{t\,mAb} - K_{t\,ss} - C_{t\,IL23})^2 + 4 \cdot C_{t\,mAb} \cdot K_{t\,ss}}}{2} \quad (32)$$

The $K_{s\,ss}$ and $K_{t\,ss}$ are the steady-state constants in serum and skin *ISF* defined as:

$$K_{s\,ss} = \frac{k_{s\,int} + k_{off}}{k_{on}} \quad (33)$$

JPET Fast Forward. Published on February 2, 2018 as DOI: 10.1124/jpet.117.244855
This article has not been copyedited and formatted. The final version may differ from this version.

$$K_{t\,ss} = \frac{k_{t\,int} + k_{off}}{k_{on}} \tag{34}$$

where the k_{on} and k_{off} refer to the ustekinumab association and dissociation rate constants against IL-23. AR_s and AR_t can be described as:

$$AR_s = C_{s\,IL23} \cdot \frac{C_{s\,fmAb}}{K_{s\,ss} + C_{s\,fmAb}} \tag{35}$$

$$AR_t = C_{t\,IL23} \cdot \frac{C_{t\,fmAb}}{K_{t\,ss} + C_{t\,fmAb}} \tag{36}$$

Model Fitting and Analysis

Model fittings and simulations were performed with NONMEM version 7.2 (ICON Development Solutions, Ellicott City, MD, USA). Naïve pooling approach was used for model fitting since data were from serial destruction and being pooled together. Between-subject variability (IIV) was not considered and the omega matrix was fixed to zero. The first-order (FO) method was used. The variance model used is

$$V_i = (\sigma_a + \sigma_p \cdot Y_i)^2 \tag{27}$$

where V_i is the variance of the *i*th observation, σ_a and σ_p are additive and proportional variance model parameters, Y_i is the *i*th model prediction. Measurements BLLOQ were treated as missing values. Model performance was evaluated by goodness-of-fit plots and objective function values (OFV). The GraphPad Prism (GraphPad Software Inc, San Diego, CA) was used for producing graphs.

Results

Serum Pharmacokinetics of CNTO 3723 (Step I)

Following 10 mg/kg IV administration, the concentration profile of CNTO 3723 in serum in healthy mice showed a bi-exponential feature with a slow terminal elimination phase (**Figure 4, Group A, symbols**). The pharmacokinetics of CNTO 3723 in normal mice in absence of any exogenous rmIL-23 dosing was first characterized with a second-generation mPBPK model.

Noncompartmental analysis (NCA) showed that CNTO 3723 exhibit approximately linear pharmacokinetics between the 3.3 - 10 mg/kg dose range, and this is consistent with the expectation for a mAb that binds to a low abundance soluble ligand. Model-fitted serum concentrations of CNTO 3723 were overlaid with the observed concentrations in healthy mice (**Figure 4, Group A**). The parameter estimates and the relative standard errors (RSE) are listed in **Table 2**. Overall, the model was able to characterize the serum concentration profiles of CNTO 3723 reasonably well. The estimated linear clearance of CNTO 3723 translates to a serum half-life about 8 days, which is in consistency with the reported serum half-life of typical murine IgGs in mice (Vieira and Rajewsky, 1988). The vascular reflection coefficient for tight tissue (σ_1) was fixed to 0.98 to obtain precise parameter estimates (Cao and Jusko, 2014). The estimated vascular reflection coefficient for leaky tissue (σ_2) is 0.657, suggesting moderate tissue distribution.

Pharmacokinetics of rmIL-23 (Step II)

The concentration profiles of rmIL-23 in serum following single IV administration in mice (**Figure 7, Group B, symbols**) showed that rmIL-23 is cleared from serum rapidly (below LLOQ within one hour). However, following ID injection in the ear, the serum concentration profile of rmIL-23 showed shallower slope (**Figure 7 Group C, symbols**), suggesting 'flip-flop' pharmacokinetics, i.e. longer apparent half-life due to the slower absorption process.

A first-generation mPBPK model was developed to describe rmIL-23 pharmacokinetics. Following ID injection, the disappearance of rmIL-23 in ear homogenates was bi-phasic (**Figure 6, Group C, symbols**). Given the low serum levels of rmIL-23, the biphasic profile of rmIL-23 in ear homogenate is most likely due to absorption from the injection site, rather than tissue distribution from central circulation. One possible physiological explanation for the observed time-dependent absorption kinetics is that the absorption kinetics is composed of a first-order regular intradermal absorption process and an initially faster absorption process, e.g. driven by increased hydrostatic pressure due to blister formation and this faster absorption process is gradually dampened as the blister heals. The model-fitted concentration profiles of rmIL-23 in

JPET Fast Forward. Published on February 2, 2018 as DOI: 10.1124/jpet.117.244855
This article has not been copyedited and formatted. The final version may differ from this version.

serum and ear homogenates and parameter estimates are listed in **Figures 6 and 7, Group B and C**, and **Table 2**. The observed concentration profiles of rmIL-23 were well-captured with this proposed parallel absorption model. The model estimated serum clearance of rmIL-23 is 307 day^{-1}, indicating rapid serum elimination (half-life about 3 min). The estimated fraction of cardiac plasma flow (Q_{CO}) for tissue *ISF* space (f_d) is 0.002, suggesting that rmIL-23 tissue distribution is diffusion rate-limited. Given the size of rmIL-23 and its hydrophilic property, it cannot readily exchange and equilibrate out between serum and tissue *ISF*. The partition coefficient (K_p) was estimated to be close to 1 during model fitting and subsequently fixed to 1, suggesting that the entire space of tissue *ISF* is available for rmIL-23 distribution. Following ear ID injection, the bioavailability (F) is low (0.0164), suggesting poor intradermal bioavailability. The estimated regular intradermal absorption rate constant (k_{abs}) is 1.88 day^{-1}, which is closed to skin lymph turnover rate (0.69 day^{-1} in human and 5.31 day^{-1} in mice when allometrically scaled with the exponent -0.25) (Ibrahim et al., 2012). This indicates that regular intradermal absorption of rmIL-23 into circulation is likely governed by the lymph flow. The first-order absorption rate constant associated with blister formation (k_{inj}) following ID injection is 53.6 day^{-1}, which is ~30-fold higher than k_{abs}. The rate constant of blister healing process (k_{dim}) is 12.3 day^{-1}, which suggests that blister heals in 4-6 hours.

Impact of Repeated ID Injections of rmIL-23 on Pharmacokinetics of CNTO 3723 and rmIL-23 (Step III)

To investigate the interaction between CNTO 3723 and rmIL-23 under psoriasis-like conditions, five repeated daily ID injections of rmIL-23 were given in mouse ear. Psoriasis-like inflammation was confirmed via ear thickness, ear weight and histopathology analysis (data not shown). Interestingly, with the daily ID injection of rmIL-23, alterations of concentration profiles of CNTO 3723 and rmIL-23 in ear homogenates were observed, which are possibly due to pathophysiological changes upon repeated rmIL-23 administration.

Impact on CNTO 3723 disposition

JPET Fast Forward. Published on February 2, 2018 as DOI: 10.1124/jpet.117.244855
This article has not been copyedited and formatted. The final version may differ from this version.

Repeated intradermal injections of rmIL-23 did not alter the systemic clearance of CNTO 3723. However, enhanced tissue uptake of CNTO 3723 into ear has been observed following administration of rmIL-23. Importantly, the concentration of CNTO 3723 exhibited transient increase immediately following each rmIL-23 ID administration (**Figure 3a**). We hypothesized that the enhanced and oscillated tissue distribution of CNTO 3723 in ear could be attributed to the increased vascular permeability and temporary cessation of the lymph propulsion following rmIL-23 ID administration. This is supported by the report that intradermal injection of inflammatory cytokines could interfere with the lymph propulsion at the injection site in mice, possibly mediated via nitric oxide pathway (Aldrich and Sevick-Muraca, 2013). The mPBPK model was modified accordingly based on this hypothesis (See Materials and Methods). The concentration profiles of CNTO 3723 in serum and ear homogenates were well-characterized with the proposed model (**Figure 4 and 5**). The estimated vascular reflection coefficients for ear skin (σ_{ear}) are 0.925 and 0.723 for healthy and PsL mice, respectively, suggesting increased vascular permeability in PsL mice compared with healthy control ones. At steady state, CNTO 3723 concentrations in ear skin *ISF* are around 10% and 25% of serum concentration in healthy and PsL mice, respectively, which are mostly consistent with the extent of tissue distribution of secukinumab in healthy subjects and psoriatic patients (23% and 28%, respectively) as determined by dermal open-flow microperfusion (dOFM) (Dragatin et al., 2016), and slightly lower than the reported skin ISF exposure for an anti-IL-17 IgG (~50%) by tissue centrifugation (Eigenmann et al., 2017). Estimated ear skin lymph turnover rate is 13 day^{-1}, which corresponds with previously measured skin lymph turnover rates (Ibrahim et al., 2012). The maximum decrease of lymph flow rate (*scal*) was estimated to be close to 1 and subsequently fixed to 0.9. The estimated lymph propulsion remission rate (d_{lym}) is 1.19 day^{-1}. Following each intradermal injection of rmIL-23, the tissue elimination rate of CNTO 3723 via lymph flow was immediately dropped to 10% and gradually recovered to 80% after 24 hours.

Impact on rmIL-23 absorption

Following repeated rmIL-23 ID administration, an apparent slower absorption of rmIL-23 from ear was observed following the 5th dose compared with the first dose, i.e., the amount of rmIL-23 remained at the injection site 24 hr after dosing was considerably higher following the 5th dose than that following the 1st dose (**Figure 3b**). One possible explanation is that the local lymph flow was damaged following repeated intradermal injections of rmIL-23. No sample was taken following the 2nd, 3rd or 4th dose, but it was reasonable to assume that this potential impact on local lymph flow was gradual. The mPBPK model was modified accordingly to reflect the change in rmIL-23 absorption process (See Materials and Methods). The change of intradermal absorption kinetics of rmIL-23 seemed to be more relevant to the repeated ID injection handling than the actual dose level of rmIL-23. In addition, the comparison of rmIL-23 concentration profiles in ear homogenates between Group C (without CNTO 3723 dosing) and Groups D – H (with CNTO 3723 dosing) following the first rmIL-23 administration showed no apparent change in the rmIL-23 absorption kinetics, indicating that the presence of CNTO 3723 did not change the absorption of rmIL-23 (**Figure 3b**). The model-fitted concentration profiles of total rmIL-23 in ear homogenates across all animal groups were shown in **Figure 6, Group D – H**. In general, the observed data were well characterized with the proposed model. The estimated ratio decrease in k_{abs} following each injection was 0.224, suggesting the lymph uptake-mediated absorption decreases 22% after each additional injection.

Interrelationship between CNTO 3723 and rmIL-23 (Step IV)

At last, the interrelationship between CNTO 3723 and rmIL-23 was characterized by overlaying the two mPBPK models for both components and including TMDD features in serum and ear skin compartments. Free rmIL-23 concentration profiles in ear homogenates and total rmIL-23 concentration profiles in serum were all applied simultaneously for model fitting. Model-fitted concentration profiles of all components well-characterize the observed measurements (**Figures 6 (red symbols and lines) and 7**). The estimated binding dissociation constant (K_D) is 0.12 nM, which is in accordance with the *in-vitro* K_D value (0.10 nM). The

JPET Fast Forward. Published on February 2, 2018 as DOI: 10.1124/jpet.117.244855
This article has not been copyedited and formatted. The final version may differ from this version.

estimated elimination rate constant of CNTO 3723-rmIL-23 binding complex in serum (k_{int}) is 0.64, which is ~7-fold higher than serum elimination rate of CNTO 3723 (serum clearance 0.0708 mL/day translates to elimination rate constant 0.083 day^{-1}).

Translational PK/PD Prediction of Ustekinumab Efficacy in Clinical Studies

To examine the potential utility of the developed mechanism-based mPBPK model in translational PK/PD, simulations of IL-23 neutralization profiles following ustekinumab treatment in psoriatic patients in various clinical studies were performed and compared with the reported clinical data. Ustekinumab binds to the common p40 subunit of IL-12 and IL-23. Given the low abundance of endogenous IL-12, the model assumed that IL-12 does not interfere with the interaction of ustekinumab and IL-23. Model also assumed that the distribution kinetics of CNTO 3723 in the ear skin in IL-23-induced PsL mice is comparable with that of ustekinumab in lesional skin site in psoriatic patients, as both mAbs have similar size and molecular structure, and human and mouse, even though with different skin counterparts (Kawamata et al., 2003), share similar vascular and interstitial tissue structure.

Model simulations were performed under various of scenarios: 1) ustekinumab given once weekly (Q1W) subcutaneously (SC) at 90 mg for four weeks as reported in a phase II clinical study (Reddy et al., 2010), 2) ustekinumab given as a single SC dose at 0.27, 0.675, 1.35 or 2.7 mg/kg as reported in a phase I clinical study (Gottlieb et al., 2007), and 3) ustekinumab 45 mg SC at 0 and 4 weeks initially, followed by 45 mg SC every 12 weeks as clinically recommended therapeutic dose for psoriatic patients weighing less than 100 kg. Related parameters values for model simulation were listed in **Table 3**. Model simulated total IL-23 concentration profiles in serum were compared with observed data, and model simulated free IL-23 concentration profiles in the lesional skin compartment were compared with reported pharmacological effect in psoriatic patients (Gottlieb et al., 2007; Reddy et al., 2010).

In the first scenario, model simulated total IL-23 concentration profile is in good agreement with measured IL-23 concentrations at different time points (**Figure 8**). Following the

escalating doses of ustekinumab (Scenario 2), model predicted free IL-23 concentration profiles in lesional skin in psoriatic patients were compared with clinically observed improvements of PASI scores as depicted in a phase I clinical study (Gottlieb et al., 2007). Interestingly, the durations of free IL-23 suppression below threshold of IL-23 baseline of healthy subjects are in accordance with the duration of sustained improvements of PASI scores, despite the small patient sample size and relatively large data variability. Lastly, model has simulated the concentration profiles of free IL-23 in serum and lesional skin sites in psoriatic patients following clinically recommended dose. Free IL-23 in lesional skin site is suppressed below the threshold of IL-23 baseline of healthy subjects during the entire time course (**Figure 9**). While on the other hand, free IL-23 in serum is suppressed to a less extent and returned to the baseline level in psoriasis patients before the next dose. This suggests that IL-23 concentration in lesional skin site correlated better with ustekinumab therapeutic efficacy.

Discussion

MAbs targeting immune cytokines are one of the most successful classes of therapeutic biologics developed for treatment of psoriasis (Tzu et al., 2008). For mAbs targeting soluble cytokines, free target suppression at the tissue site of action is anticipated to be a driver for all downstream pharmacologic effect and therapeutic efficacy, and thus can be a highly valuable translational biomarker. However, free cytokine levels can be technically difficult to determine, especially for the ones with low baseline or function at tissue sites. Moreover, free cytokine suppression at tissue sites cannot be simply extrapolated from that in blood as both the cytokines and the mAbs targeting them are expected to exhibit entirely different kinetics at tissue sites and in blood.

In order to understand target engagement for mAbs against cytokines function at tissue sites, a mechanism-based mPBPK model with TMDD features incorporated in both serum and ear skin was developed to characterize the relationship between CNTO 3723 and rmIL-23 in an IL-23-induced PsL mouse model. The translational utility of this model was examined using

ustekinumab. The mPBPK model derived mAb and IL-23 tissue distribution and kinetics parameters were combined with other system- and drug-specific properties such as IL-23 baseline in psoriatic patients, ustekinumab human PK, and IL-23 binding affinity for ustekinumab to predict free IL-23 suppression in skin lesion in psoriatic patients. The results corroborated reasonably well with the observed clinical data, demonstrating the potential of our approach in translational research at the preclinical-clinical interface.

The mPBPK model in PsL mice was developed in a stepwise process which quantitatively delineates each step in the causal chain of the exposure-response relationship of CNTO 3723 and IL-23 at the tissue site of action: 1) tissue distribution of CNTO 3723 to the lesional skin sites, 2) IL-23 dynamics at the lesional skin sites, 3) IL-23 binding and disposition at the target tissue site, and 4) free IL-23 suppression in the lesional skin. Development of a mPBPK model with TMDD features in both blood and tissue requires measurements of the CNTO 3723 and free/total IL-23 concentrations. Endogenous IL-23 is expressed at extremely low levels, i.e., below the limit of quantification of all known bioanalytical method, making it challenging to study endogenous IL-23 target engagement. To overcome this challenge, exogenously administered rmIL-23 was used. Repeated intradermal administration of rmIL-23 in mice not only led to establishment of a psoriasis-like mouse model, it boosts rmIL-23 baseline concentrations in both serum and ear skin tissues to enable the measurement of rmIL-23 target engagement. Even though rmIL-23 levels in this model are not physiological, they allow us to characterize the physiological processes including mAb disposition, IL-23 kinetics, and the interaction between mAb and IL-23. The information can then be integrated with the physiological levels of IL-23 in psoriatic patients to predict therapeutic effect of anti-IL-23 mAbs in humans.

Interestingly, our results showed that free IL-23 suppression at tissue sites can be more effective than that in blood despite the lower mAb level and higher IL-23 level at the tissue site. This can be attributed to the substantially lower mAb-IL-23 complex accumulation at the tissue

site. In blood, IL-23 is subject to rapid elimination (half-life in minutes) while mAb-IL-23 complex is eliminated much slower (half-life in days, similar to that of IgG). This leads to a rapid accumulation of total IL-23 in blood after mAb dosing. The mAb-IL-23 complex would dissociate and form a new equilibrium between mAb and free IL-23, resulting in return of free IL-23 to baseline level when the mAb concentrations are still orders of magnitude higher (Wang et al., 2014). On the other hand, free IL-23 and mAb-IL-23 complex have similar elimination rates (close to that of lymph drainage) at the tissue site and there is minimal accumulation of mAb-IL-23 complex, resulting in more effective free IL-23 suppression in the ear skin.

In our mPBPK model, the pharmacokinetics of rmIL-23 and CNTO 3723 were characterized with the first- and second-generation mPBPK model, respectively (Cao and Jusko, 2012; Cao et al.,2013). Compared to mAbs, rmIL-23 exhibits more rapid and extensive tissue distribution. The 'first-generation' mPBPK model, which assumes whole tissue weight or tissue interstitial space as the extravascular distribution space and tissue distribution is driven by Fick's Law of diffusion, is found to be more suitable for describing the disposition of rmIL-23. The 'second-generation' mPBPK model was developed with considerations of specific PK characteristics of mAbs, i.e. only convection is considered as the driver for extravascular distribution, and only ISF is considered as the extravascular distribution space, and it was used to describe the disposition of CNTO 3723. Importantly, both the first- and second-generation mPBPK models used physiological volumes and flows, and thus could be easily integrated for assessing the interrelationship between CNTO 3723 and IL-23.

A vascular endothelial endosome space and FcRn-mAb interaction are frequently included in PBPK models for mAbs to assess the influence of FcRn interaction (Garg and Balthasar, 2007; Chetty et al., 2014). Since our interest focused on understanding the target engagement at tissue site of action, not the impact of FcRn binding, they are not included in our mPBPK model. It should be noted that the overall volume of vascular endothelial endosomes was only about 0.4% of plasma and less than 0.1% of ISF volume (Cao et al.,2013), so the

JPET Fast Forward. Published on February 2, 2018 as DOI: 10.1124/jpet.117.244855
This article has not been copyedited and formatted. The final version may differ from this version.

contribution of mAbs reside within this space to overall mAb disposition is expected to be limited at any moment of time. In addition, FcRn-mediated clearance (i.e. salvage of mAbs following their pinocytosis) and extravascular distribution are both linear processes unless the mAb concentrations are greater than ~10 mg/mL (Roopenian and Akilesh, 2007). Therefore, the linear serum clearance and extravascular distribution functions implemented in our mPBPK model would implicitly include these FcRn-mediated mechanisms.

Two important physiological determinants that describe the distribution kinetics of CNTO 3723 into ear skin are transvascular fluid flux rate, which would equal lymph flow rate (L) based on fluid mass balance, and vascular permeability (σ). Lymph flow rate is commonly determined through lymph node cannulation, but skin is the largest organ that covers the entire body and skin lymph flow rate cannot be assessed directly. Instead of lymph flow rate, the lymph turnover rate of skin (k_{ear}) is applied. The k_{ear} is defined as L divided by ISF volume (V_{ISF}), and could be measured experimentally by tracing the removal rate of radioactive-labelled albumin (Reed et al., 1985). The estimated regular intradermal absorption rate constant of rmIL-23 is also comparable with the reported skin lymph turnover rate, suggesting the regular intradermal absorption pathway for IL-23 is predominantly lymph uptake. Besides the regular intradermal absorption, absorption of rmIL-23 following ID injection was also impacted by blister-formation. Similar to that following subcutaneous (SC) administration, large molecule absorption following ID injection is driven by the differences in hydrostatic and osmotic pressure between blood circulation, interstitium and the lymphatic vessels (Wiig and Swartz, 2012). Blister formed due to repeated intradermal injection of rmIL-23 increases hydrostatic pressure in the interstitium, which might cause rapid absorption of rmIL-23 into capillaries. It has been observed that ID administration of proteins produced higher maximum serum concentration (C_{max}) and a 'left-shift' in serum concentration profiles comparing to the SC route (Milewski et al., 2015).

For our PsL mice study, it was unexpected to find that repeated ID administration of a relatively large volume of rmIL-23 to the mouse ears led to certain pathophysiological changes

that affected the pharmacokinetics of CNTO 3723 as well as rmIL-23. This presented challenges in directly using results from the PsL mouse model for human dose projection, because such effects are not expected to happen in humans. One advantage of using a mechanism and physiologically based model is that the model can be expanded with additional components corresponding to possible physiological explanations to capture the observed data for CNTO 3723 and IL-23 in both serum and skin. Since the model distinguished the effects from "physiological" and "non-physiological" processes, only the physiological one was used for human dose projection.

In conclusion, we provided a good case example on how mechanism and physiologically based modeling and simulations can be applied during early drug discovery and preclinical to clinical translational stages. Simple extrapolation of drug exposure-efficacy relationship from preclinical species to human likely will not work due to the inter-species differences in disease status, target kinetics and drug disposition. In particular, tissue specific drug and target kinetics information must be considered to understand target suppression at the tissue site of action. Physiologically-based PK/PD modeling can be an invaluable tool to understand system-specific and drug-specific physiological parameters to enable successful translation from preclinical models to humans.

Acknowledgements

We would like to thank Natasha Rozenkrants for helping to establish the IL-23-induced PsL model. Dr. Yang Wang for helping managing the in-life study conducted at WuXi Apptec.

Authorship Contributions

Participated in research design: XC, JX, HZ, WW

Conducted experiments: XC, RD, BG, TM, WW

Contributed new reagents or analytical tools: XC, RD, BG, TM

Performed data analysis: XC, JX, HZ, WW

Wrote or contributed to the writing of the manuscript: XC, JX, RD, BG, TM, WJJ, HZ, WW

References

Agoram BM, Martin SW and van der Graaf PH (2007) The role of mechanism-based pharmacokinetic-pharmacodynamic (PK-PD) modelling in translational research of biologics. *Drug Discov Today* **12**:1018-1024.

Aldrich MB and Sevick-Muraca EM (2013) Cytokines are systemic effectors of lymphatic function in acute inflammation. *Cytokine* **64**:362-369.

Arican O, Aral M, Sasmaz S and Ciragil P (2005) Serum levels of TNF-alpha, IFN-gamma, IL-6, IL-8, IL-12, IL-17, and IL-18 in patients with active psoriasis and correlation with disease severity. *Mediators Inflamm* **2005**:273-279.

Campa M, Mansouri B, Warren R, Menter A (2016) A Review of Biologic Therapies Targeting IL-23 and IL-17 for Use in Moderate-to-Severe Plaque Psoriasis. *Dermatol Ther (Heidelb)*.**6**:1-12.

Cao Y, Balthasar JP and Jusko WJ (2013) Second-generation minimal physiologically-based pharmacokinetic model for monoclonal antibodies. *J Pharmacokinet Pharmacodyn* **40**:597-607.

Cao Y and Jusko WJ (2012) Applications of minimal physiologically-based pharmacokinetic models. *J Pharmacokinet Pharmacodyn* **39**:711-723.

Cao Y and Jusko WJ (2014) Incorporating target-mediated drug disposition in a minimal physiologically-based pharmacokinetic model for monoclonal antibodies. *J Pharmacokinet Pharmacodyn* **41**:375-387.

Chan JR, Blumenschein W, Murphy E, Diveu C, Wiekowski M, Abbondanzo S, Lucian L, Geissler R, Brodie S, Kimball AB, Gorman DM, Smith K, de Waal Malefyt R, Kastelein RA, McClanahan TK and Bowman EP (2006) IL-23 stimulates epidermal hyperplasia via

TNF and IL-20R2-dependent mechanisms with implications for psoriasis pathogenesis. *J Exp Med* **203**:2577-2587.

Chen X, Jiang X, Jusko WJ, Zhou H and Wang W (2016) Minimal physiologically-based pharmacokinetic (mPBPK) model for a monoclonal antibody against interleukin-6 in mice with collagen-induced arthritis. *J Pharmacokinet Pharmacodyn* **43**:291-304.

Chetty M, Li L, Rose R, Machavaram K, Jamei M, Rostami-Hodjegan A, Gardner I. (2015) Prediction of the Pharmacokinetics, Pharmacodynamics, and Efficacy of a Monoclonal Antibody, Using a Physiologically Based Pharmacokinetic FcRn Model. *Front Immunol*. **5**:670.

Danhof M, de Jongh J, De Lange EC, Della Pasqua O, Ploeger BA and Voskuyl RA (2007) Mechanism-based pharmacokinetic-pharmacodynamic modeling: biophase distribution, receptor theory, and dynamical systems analysis. *Annu Rev Pharmacol Toxicol* **47**:357-400.

Dong J and Goldenberg G (2017) New biologics in psoriasis: an update on IL-23 and IL-17 inhibitors. *Cutis* **99**:123-127.

Dragatin C, Polus F, Bodenlenz M, Calonder C, Aigner B, Tiffner KI, Mader JK, Ratzer M, Woessner R, Pieber TR, Cheng Y, Loesche C, Sinner F and Bruin G (2016) Secukinumab distributes into dermal interstitial fluid of psoriasis patients as demonstrated by open flow microperfusion. *Exp Dermatol* **25**:157-159.

Eigenmann MJ, Karlsen TV, Krippendorff BF, Tenstad O, Fronton L, Otteneder MB and Wiig H (2017) Interstitial IgG antibody pharmacokinetics assessed by combined in vivo- and physiologically-based pharmacokinetic modelling approaches. *J Physiol*.

El Hadidi H GB, Gheita T, Shaker O (2008) Involvement of IL-23 in psoriasis and psoriatic arthritis patients; possible role in pathogenesis. *J Egypt worn Dermatol Soc* **5**:70-76.

Garg A, Balthasar JP (2007) Physiologically-based pharmacokinetic (PBPK) model to predict IgG tissue kinetics in wild-type and FcRn-knockout mice. *J Pharmacokinet Pharmacodyn.* **34**:687–709.

Gibiansky L, Gibiansky E, Kakkar T and Ma P (2008) Approximations of the target-mediated drug disposition model and identifiability of model parameters. *Journal of pharmacokinetics and pharmacodynamics* **35**:573-591.

Gottlieb AB, Cooper KD, McCormick TS, Toichi E, Everitt DE, Frederick B, Zhu Y, Pendley CE, Graham MA and Mascelli MA (2007) A phase 1, double-blind, placebo-controlled study evaluating single subcutaneous administrations of a human interleukin-12/23 monoclonal antibody in subjects with plaque psoriasis. *Curr Med Res Opin* **23**:1081-1092.

Hu C, Wasfi Y, Zhuang Y and Zhou H (2014) Information contributed by meta-analysis in exposure-response modeling: application to phase 2 dose selection of guselkumab in patients with moderate-to-severe psoriasis. *J Pharmacokinet Pharmacodyn* **41**:239-250.

Ibrahim R, Nitsche JM and Kasting GB (2012) Dermal clearance model for epidermal bioavailability calculations. *J Pharm Sci* **101**:2094-2108.

Kawamata S, Ozawa J, Hashimoto M, Kurose T and Shinohara H (2003) Structure of the rat subcutaneous connective tissue in relation to its sliding mechanism. *Arch Histol Cytol* **66**:273-279.

Kopp T, Lenz P, Bello-Fernandez C, Kastelein RA, Kupper TS and Stingl G (2003) IL-23 production by cosecretion of endogenous p19 and transgenic p40 in keratin 14/p40 transgenic mice: evidence for enhanced cutaneous immunity. *J Immunol* **170**:5438-5444.

Lima HC and Kimball AB (2010) Targeting IL-23: insights into the pathogenesis and the treatment of psoriasis. *Indian J Dermatol* **55**:171-175.

Lowes MA, Russell CB, Martin DA, Towne JE and Krueger JG (2013) The IL-23/T17 pathogenic axis in psoriasis is amplified by keratinocyte responses. *Trends Immunol* **34**:174-181.

McLennan DN, Porter CJ and Charman SA (2005) Subcutaneous drug delivery and the role of the lymphatics. *Drug Discov Today Technol* **2**:89-96.

Milewski M, Manser K, Nissley BP and Mitra A (2015) Analysis of the absorption kinetics of macromolecules following intradermal and subcutaneous administration. *Eur J Pharm Biopharm* **89**:134-144.

Nestle FO, Kaplan DH and Barker J (2009) Psoriasis. *N Engl J Med* **361**:496-509.

Reddy M, Torres G, McCormick T, Marano C, Cooper K, Yeilding N, Wang Y, Pendley C, Prabhakar U, Wong J, Davis C, Xu S and Brodmerkel C (2010) Positive treatment effects of ustekinumab in psoriasis: analysis of lesional and systemic parameters. *J Dermatol* **37**:413-425.

Reed RK, Johansen S and Noddeland H (1985) Turnover rate of interstitial albumin in rat skin and skeletal muscle. Effects of limb movements and motor activity. *Acta Physiol Scand* **125**:711-718.

Rizzo HL, Kagami S, Phillips KG, Kurtz SE, Jacques SL and Blauvelt A (2011) IL-23-mediated psoriasis-like epidermal hyperplasia is dependent on IL-17A. *J Immunol* **186**:1495-1502.

Roopenian DC, Akilesh S. (2007) FcRn: the neonatal Fc receptor comes of age. *Nat Rev Immunol*. **7**:715-25.Schon MP and Boehncke WH (2005) Psoriasis. *N Engl J Med* **352**:1899-1912.

Shah DK and Betts AM (2012) Towards a platform PBPK model to characterize the plasma and tissue disposition of monoclonal antibodies in preclinical species and human. *Journal of pharmacokinetics and pharmacodynamics* **39**:67-86.

Vieira P and Rajewsky K (1988) The half-lives of serum immunoglobulins in adult mice. *Eur J Immunol* **18**:313-316.

Wang W, Wang X, Doddareddy R, Fink D, McIntosh T, Davis HM, Zhou H (2014) Mechanistic pharmacokinetic/target engagement/pharmacodynamic (PK/TE/PD) modeling in deciphering interplay between a monoclonal antibody and its soluble target in cynomolgus monkeys. *AAPS J*. **16**:129-39.

Wiig H and Swartz MA (2012) Interstitial fluid and lymph formation and transport: physiological regulation and roles in inflammation and cancer. *Physiol Rev* **92**:1005-1060.

Zhou H, Hu C, Zhu Y, Lu M, Liao S, Yeilding N and Davis HM (2010) Population-based exposure-efficacy modeling of ustekinumab in patients with moderate to severe plaque psoriasis. *J Clin Pharmacol* **50**:257-267.

Zhu YW, Mendelsohn A, Pendley C, Davis HM and Zhou H (2010) Population pharmacokinetics of ustekinumab in patients with active psoriatic arthritis. *Int J Clin Pharmacol Ther* **48**:830-846.

Figure Legends

Figure 1. Scheme of mPBPK models with TMDD features developed step-wise for characterization of distribution of CNTO 3723 and its interrelationship with rmIL-23 in serum and ear skin in IL-23-induced PsL mice. **a)** Second-generation mPBPK model applied for the characterization of serum pharmacokinetics of CNTO 3723 in Step I, **b)** First-generation mPBPK model applied for the characterization pharmacokinetics of rmIL-23 in Step II, **c)** Second-generation mPBPK model including ear skin tissue compartment for the characterization of distribution of CNTO 3723 to ear skin in Step III, and **d)** First- and second-generation mPBPK models overlaid with TMDD features incorporated in serum and ear skin compartments for the characterization of the interplay between CNTO 3723 and rmIL-23 in Step IV.

Figure 2. Scheme of translational PK/PD model applied for ustekinumab pharmacological effect prediction in psoriatic patients.

Figure 3. Alterations of concentration profiles CNTO 3723 and rmIL-23 in ear homogenates following repeated IL-23 ID treatment. **a**) CNTO 3723 concentration profiles in ear homogenates in all treatment groups. Compared with non-treated animals (Group A), at the same CNTO3723 doses, enhanced CNTO 3723 ear distribution was observed following ID treatment with rmIL-23 (Group F and H). Also, immediately following rmIL-23 ID treatment, the ear concentration of CNTO3723 showed transient increase when comparing CNTO 3723 concentration at day 3 (right before the second rmIL-23 dose) and day 6 (immediately after the fifth rmIL-23 dose). **b**) rmIL-23 concentration profiles in ear homogenates in all treatment groups. The concentration profiles following the first rmIL-23 ID dose with concurrent CNTO 3723 treatment in

Group D – H showed similar kinetics with that following rmIL-23 treatment alone (Group C). Also, following the fifth ID dose (day 6 – 7), rmIL-23 showed slower clearance in ear compared with that following the first dose (day 2 – 3).

Figure 4. Model-fitted Serum CNTO 3723 concentrations versus time profiles. Circles are measured concentrations, and curves depict model fittings.

Figure 5. Model-fitted CNTO 3723 concentrations versus time profiles in ear homogenates. Circles are measured concentrations, and curves depict model fittings.

Figure 6. Model-fitted rmIL-23 concentrations versus time profiles in ear homogenates. Blue circles are measured total rmIL-23 concentrations, red circles are measured free rmIL-23 concentrations, curves depict model fittings, and arrows indicate the first and last rmIL-23 administration.

Figure 7. Model-fitted rmIL-23 concentrations versus time profiles in serum. Blue circles are measured total rmIL-23 concentrations, curves depict model fittings, and arrows indicate the first and last rmIL-23 administration.

Figure 8. Model predicted total IL-23 concentration-time profiles in serum overlaid with measured IL-23 serum concentrations following SC administration of ustekinumab Q1W for 4 weeks. Triangles are measured IL-23 serum concentrations and curves depict model predictions.

Figure 9. a) Model predicted free IL-23 concentration-time profiles in lesional skin following single escalating SC administration of overlaid with measured IL-23 serum concentrations following SC administration of ustekinumab (placebo, 0.27, 0.675, 1.35 and 2.7 mg/kg). Curves represent model predictions and dashed and solid gray lines are baseline concentrations of IL-23 in psoriatic patients and healthy subjects. **b**) Model

predicted free IL-23 concentration-time profiles in serum and lesional skin following clinical recommended therapeutic dose (45 mg SC at 0 and 4 weeks initially, followed by 45 mg SC every 12 weeks). Curves depict model predictions and dashed and solid gray lines are baseline concentrations of IL-23 in psoriatic patients and healthy subjects in serum and lesional skin.

JPET Fast Forward. Published on February 2, 2018 as DOI: 10.1124/jpet.117.244855
This article has not been copyedited and formatted. The final version may differ from this version.

Table 1. Animal study scheme

Grp	Dose		Number of animals (N)	Sampling time point	
	CNTO3723 (mg/kg)	rmIL-23 (ng)		Retro-orbital	Terminal
A	10	NA	12 (4 × 3/ea)	15 min, 6 h, 1, 2, 7 and 17 days	2 h, 2, 14 and 21 days (n=3/ea)
B	NA	400	16 (4 × 4/ea)	15 min, 2 and 6 h, 3 days	1 h, 1, 2, and 5 days
C	NA	400	24 (6 × 4/ea)	30 min, 1 and 8 h, 1 and 3 days	15 min, 2 and 6 h, 1, 2 and 5 days
D	3.3	50	45 (9 × 5/ea)	1, 4 and 8 h after first IL-23 dose; 1 and 8 h after the fifth IL-23 dose; 5, 8 and 17 days	2 and 24 h after the first IL-23 dose; 0, 2, 4, and 24 h after the fifth IL-23 dose; 9, 13 and 22 days
E	3.3	200	45 (9 × 5/ea)		
F	10	200	45 (9 × 5/ea)		
G	3.3	500	45 (9 × 5/ea)		
H	10	200	20 (4 × 5/ea)	1 and 24 h post CNTO 3723 dose on day 0; 0 h pre- and 24 h post IL-23 dose on day 2	5 and 15 min, 1 and 24 h post IL-23 dose on day 2

JPET Fast Forward. Published on February 2, 2018 as DOI: 10.1124/jpet.117.244855
This article has not been copyedited and formatted. The final version may differ from this version.

Table 2. Summary of model parameters and estimates

Parameter	Definition	Estimate	RSE(%)
	Step I: Pharmacokinetics of CNTO 3723		
σ_1	Vascular reflection coefficient of tight tissue	0.98	Fixed
σ_2	Vascular reflection coefficient of leaky tissue	0.657	8
CL_{ctrl} (mL/day)	Linear serum clearance	0.0708	14
	Step II: Pharmacokinetics of rmIL-23		
f_d	Fraction of Q_{CO} for V_t	0.0023	10
K_p	Partition coefficient	1	Fixed
$CL_{s\ IL23}$ (mL/day)	Linear serum clearance	307	8
F	Bioavailability	0.0164	11
k_{abs} (1/day)	Regular ID absorption rate constant	1.88	38
k_{inj} (1/day)	Absorption rate constant from ID caused by blister formation	53.6	19
k_{dim} (1/day)	Rate constant of blister healing process	12.3	31
	Step III: Pharmacokinetics Alteration of rmIL-23 and CNTO 3723		
	Alteration of rmIL-23 Pharmacokinetics		
fac_{lym}	Ratio decrease in k_{abs} following each rmIL-23 ID dose	0.224	7
	Alteration of CNTO 3723 Pharmacokinetics		
σ_{ear_ctrl}	Vascular reflection coefficient of ear in healthy mice	0.925	1
σ_{ear_PsL}	Vascular reflection coefficient of ear in PsL mice	0.723	9
k_{ear} (1/day)	Ear lymph flow turnover rate	13	38
scal	Maximum ratio decrease in lymph flow rate	0.9	Fixed
d_{lym} (1/day)	Remission rate of lymph propulsion	1.19	12
	Step IV: Interrelationship between CNTO 3723 and rmIL-23		
K_D (nM)	Binding dissociation coefficient	0.12	55
k_{int} (1/day)	Elimination rate constant of complex in serum	0.65	24
	Physiological parameters of mouse (25 g)		
V_s (mL)[a]	Serum volume	0.85	
ISF (mL) [a]	Total tissue interstitial space volume	4.35	
V_{lymph} (mL) [a]	Lymph volume	1.53	
L (mL/day)[b]	Total lymph flow rate	2.88	
Q_{CO} (mL/day)[c]	Cardiac plasma flow rate	20950	

[a] Physiological parameter values obtained from (Shah and Betts, 2012). Assumed 25 g body weight

[b] Total lymphatic flow allometrically scaled from human (2.9 L/day) with exponent factor 0.74.

[c] Physiological parameter values obtained from (Shah and Betts, 2012). Assumed 25 g body weight.

JPET Fast Forward. Published on February 2, 2018 as DOI: 10.1124/jpet.117.244855
This article has not been copyedited and formatted. The final version may differ from this version.

Table 3. Model parameters for simulation

Parameter	Definition	Value
Ustekinumab serum pharmacokinetics[a]		
k_a (1/day)	First-order absorption rate constant follow SC administration	0.354
V/F (L)	Apparent volume of distribution	15.7
CL/F (L/day)	Apparent clearance	0.465
Ustekinumab tissue distribution kinetics[b]		
σ_{skin}	Vascular reflection coefficient of lesional skin sites	0.742
σ_L	Lymph reflection coefficient of lesional skin sites	0.2
k_{skin} (1/day)	Lymph flow turnover rate of skin	1.4
IL-23 baseline concentration[a]		
$C_{s\ IL23b}$ (pg/mL)	Serum baseline concentration of IL-23 in psoriatic patients	38.5
$C_{Hs\ IL23b}$ (pg/mL)	Serum baseline concentration of IL-23 in healthy subjects	24
$C_{t\ IL23b}$ (pg/mL)	Skin baseline concentration of IL-23 in psoriatic patients	2200
$C_{Ht\ IL23b}$ (pg/mL)	Skin baseline concentration of IL-23 in healthy subjects	936
Ustekinumab interaction with IL-23[b]		
$k_{s\ deg}$ (1/day)	Serum degradation rate constant of IL-23	39.8
$k_{s\ syn}$ (nM/day)	Serum synthesis rate of IL-23	0.028
$k_{s\ int}$ (1/day)	Elimination rate constant of complex in serum	0.15
$k_{t\ deg}$ (1/day)	Skin degradation rate constant of IL-23	2.8
$k_{t\ syn}$ (nM/day)	Skin synthesis rate of IL-23	0.112
$k_{t\ int}$ (1/day)	Elimination rate constant of complex in skin	1.4

[a] Parameter values obtained from (El Hadidi H, 2008; Zhu et al., 2010).

[b] Parameter values estimated based on allometric scaling from mice. σ_{skin} and σ_L assumed the same from mice, k_{skin} and $k_{s\ deg}$ allometrically scaled from mice with exponent factor -0.25, $k_{t\ deg}$ assumed 2-fold of skin lymph turnover rate (k_{skin}) (Chen et al., 2016), $k_{s\ syn}$ and $k_{t\ syn}$ calculated by multiplying degradation rate constant with IL-23 baseline concentrations, $k_{s\ int}$ assumed 7-fold of ustekinumab elimination rate constant (CL/V) based on model fitting exercise, and $k_{t\ int}$ assumed the same with skin lymph turnover rate (k_{skin}) (Chen et al., 2016).

JPET Fast Forward. Published on February 2, 2018 as DOI: 10.1124/jpet.117.244855
This article has not been copyedited and formatted. The final version may differ from this version.

Figure 1

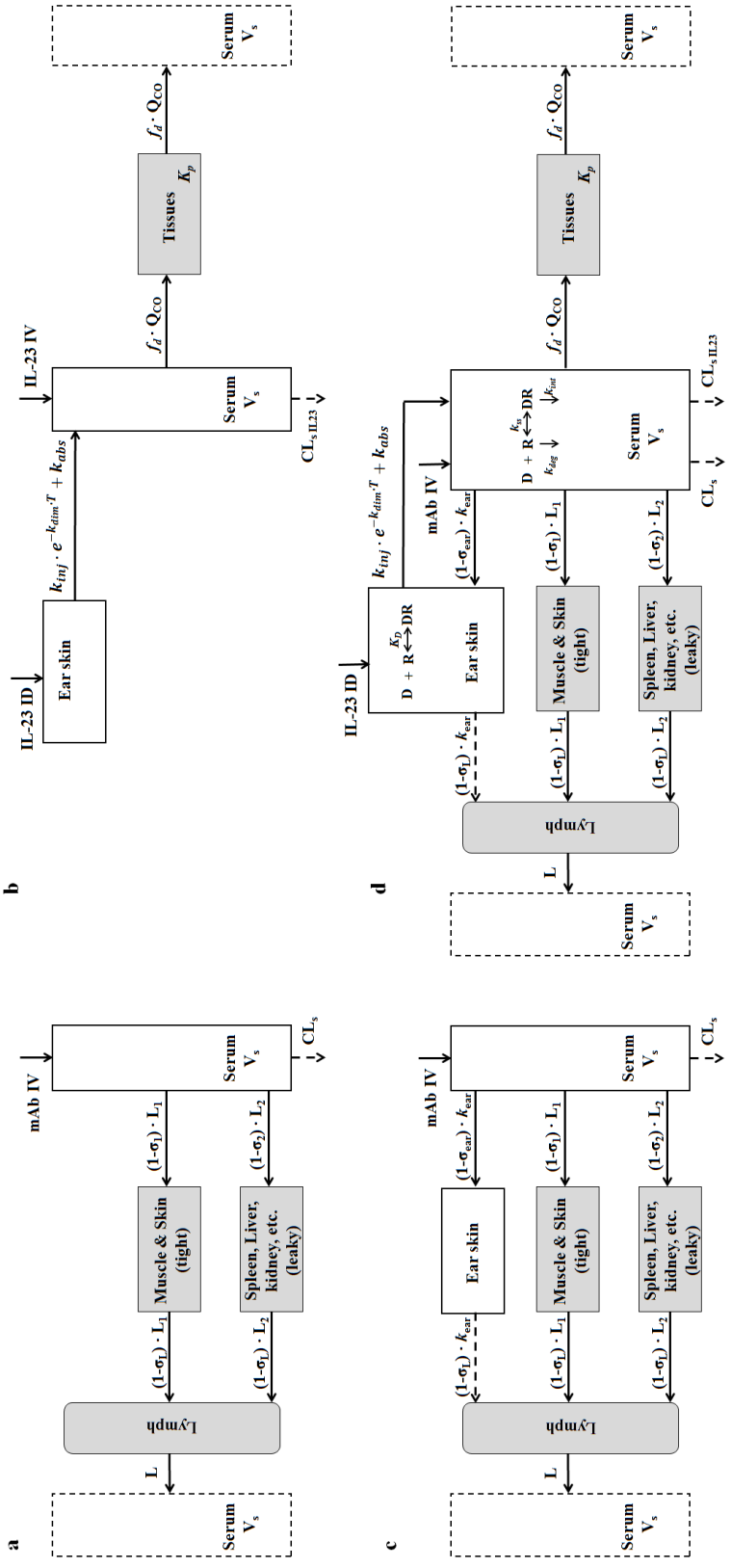

JPET Fast Forward. Published on February 2, 2018 as DOI: 10.1124/jpet.117.244855
This article has not been copyedited and formatted. The final version may differ from this version.

Figure 2

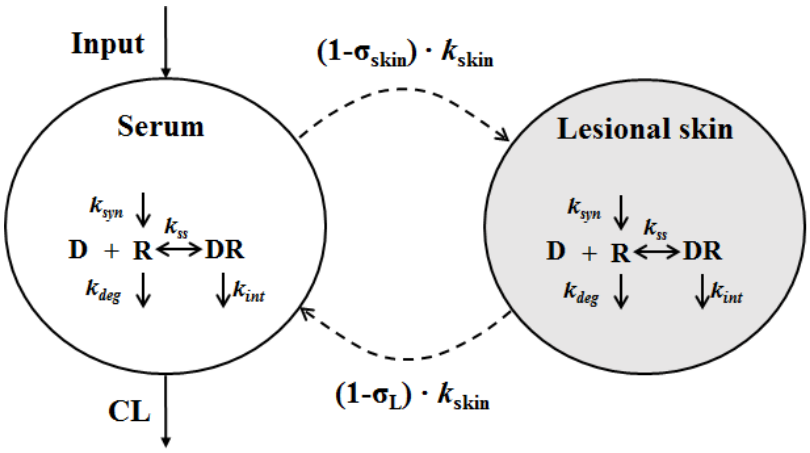

JPET Fast Forward. Published on February 2, 2018 as DOI: 10.1124/jpet.117.244855
This article has not been copyedited and formatted. The final version may differ from this version.

Figure 3

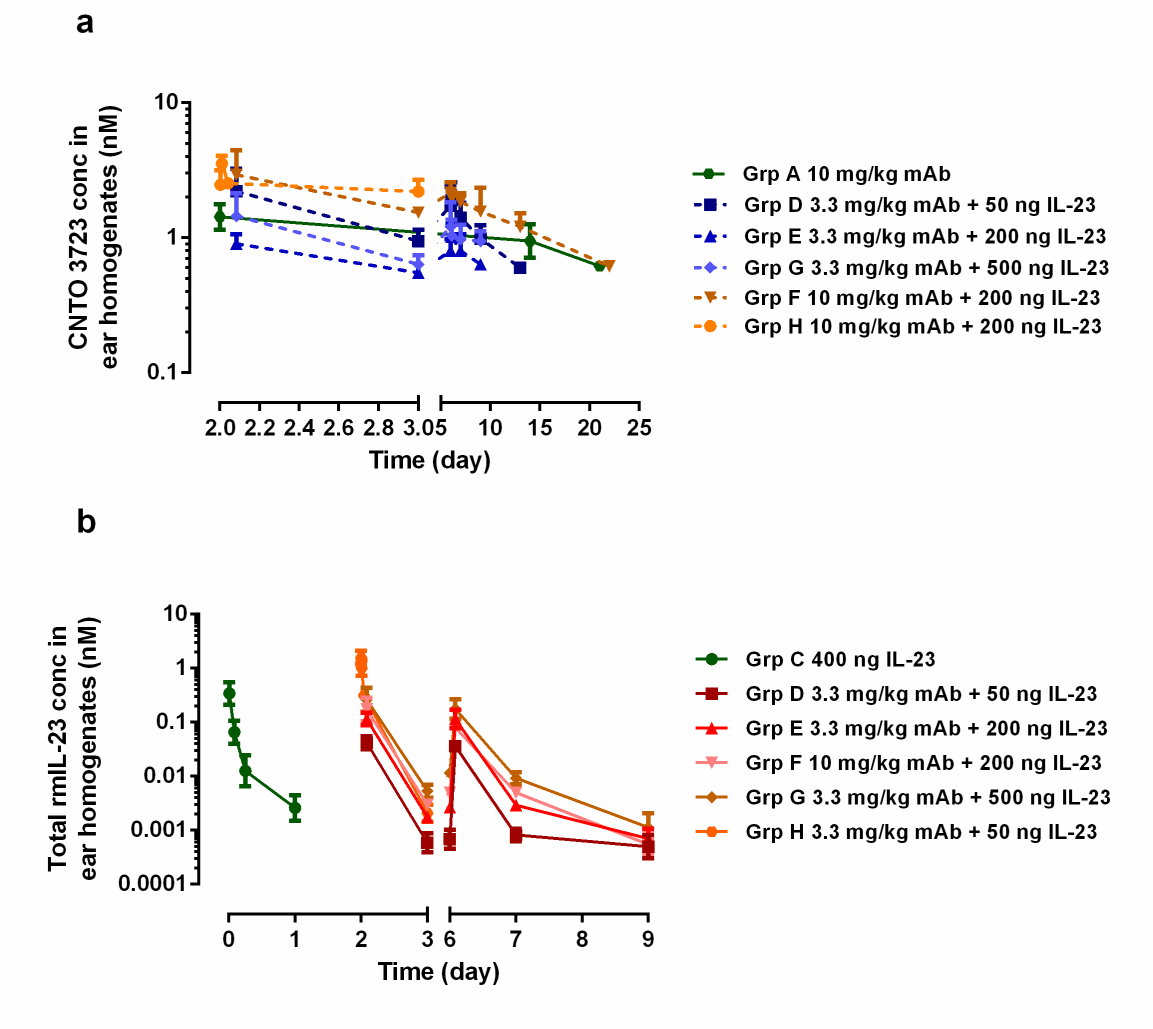

JPET Fast Forward. Published on February 2, 2018 as DOI: 10.1124/jpet.117.244855
This article has not been copyedited and formatted. The final version may differ from this version.

Figure 4

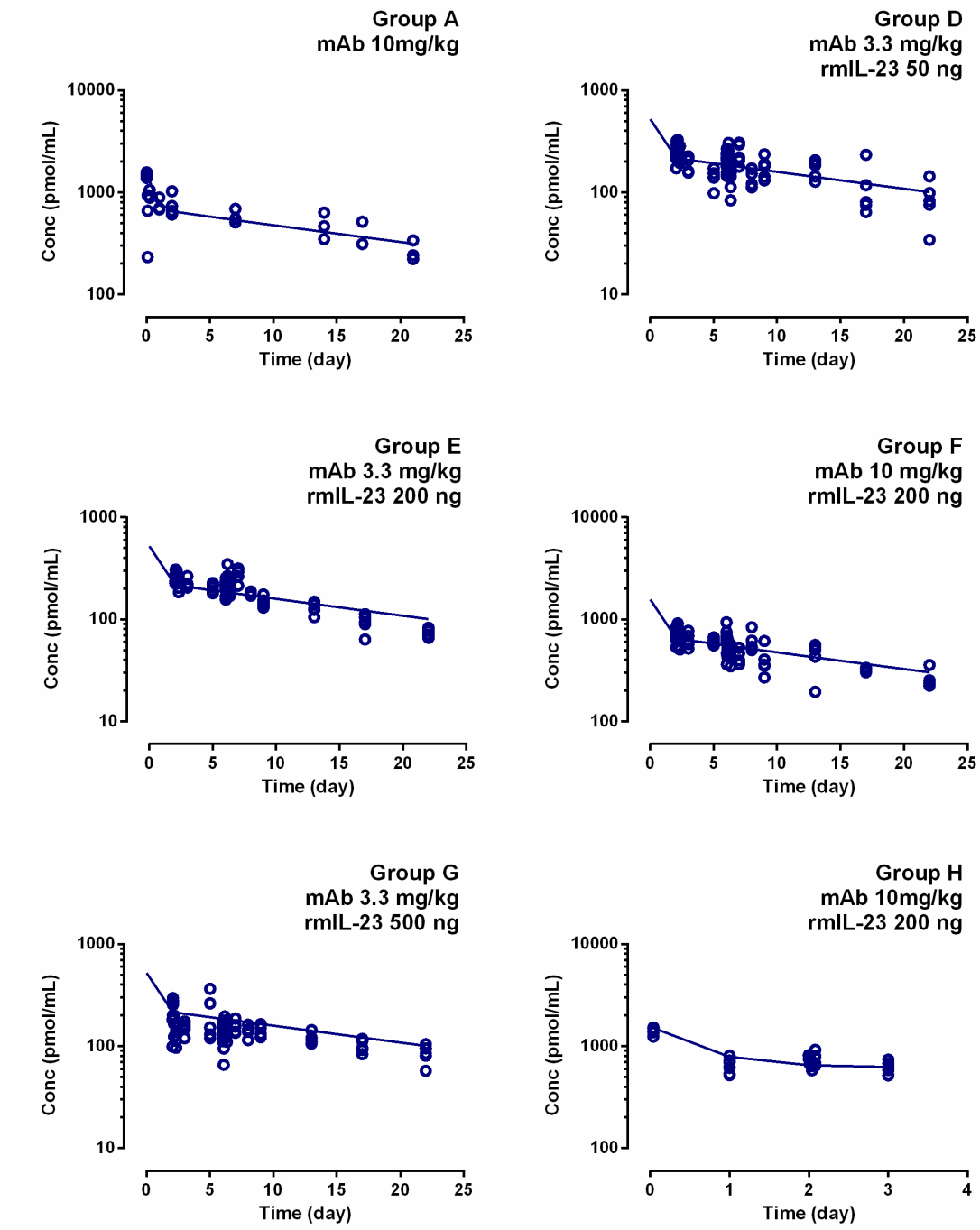

JPET Fast Forward. Published on February 2, 2018 as DOI: 10.1124/jpet.117.244855
This article has not been copyedited and formatted. The final version may differ from this version.

Figure 5

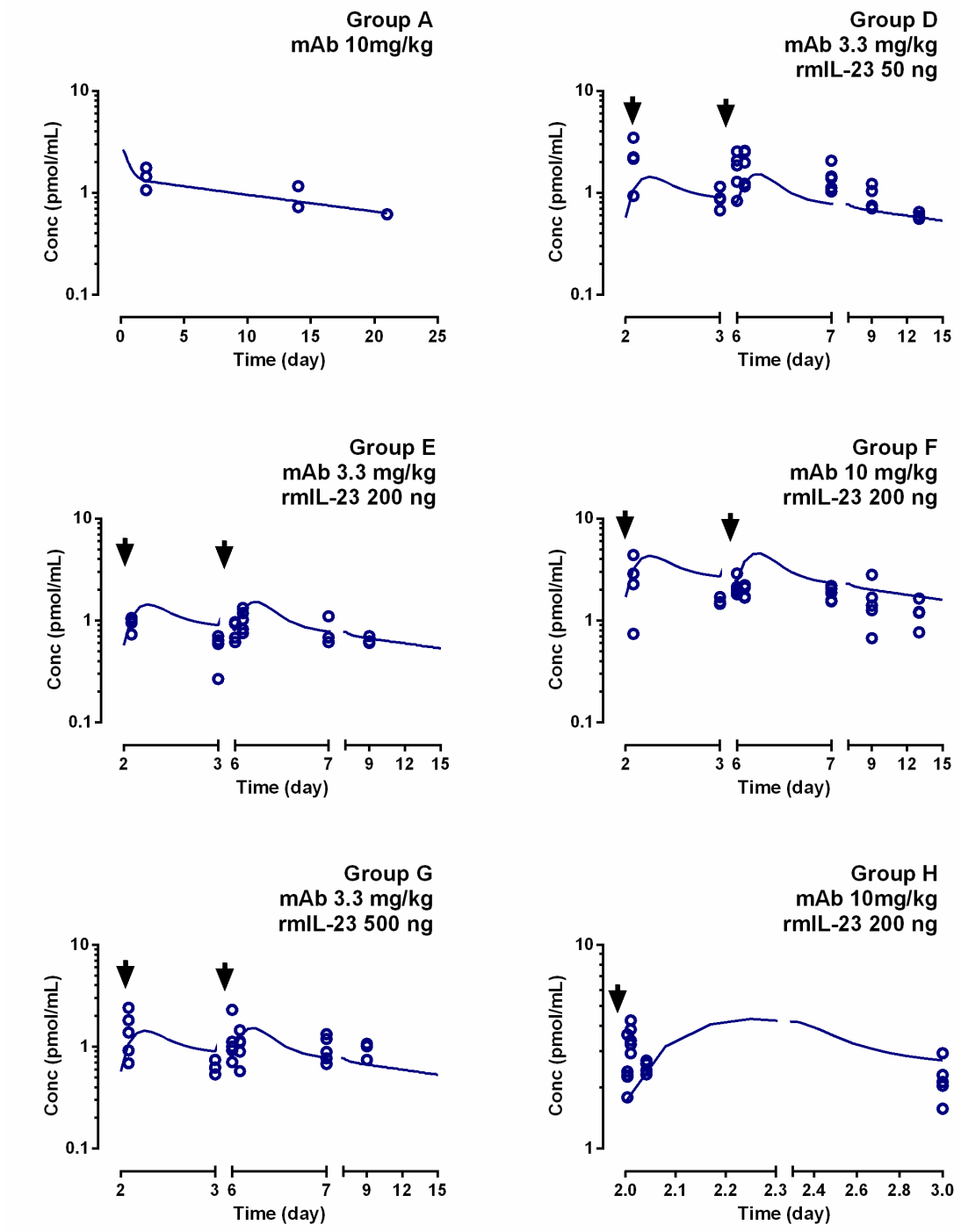

JPET Fast Forward. Published on February 2, 2018 as DOI: 10.1124/jpet.117.244855
This article has not been copyedited and formatted. The final version may differ from this version.

Figure 6

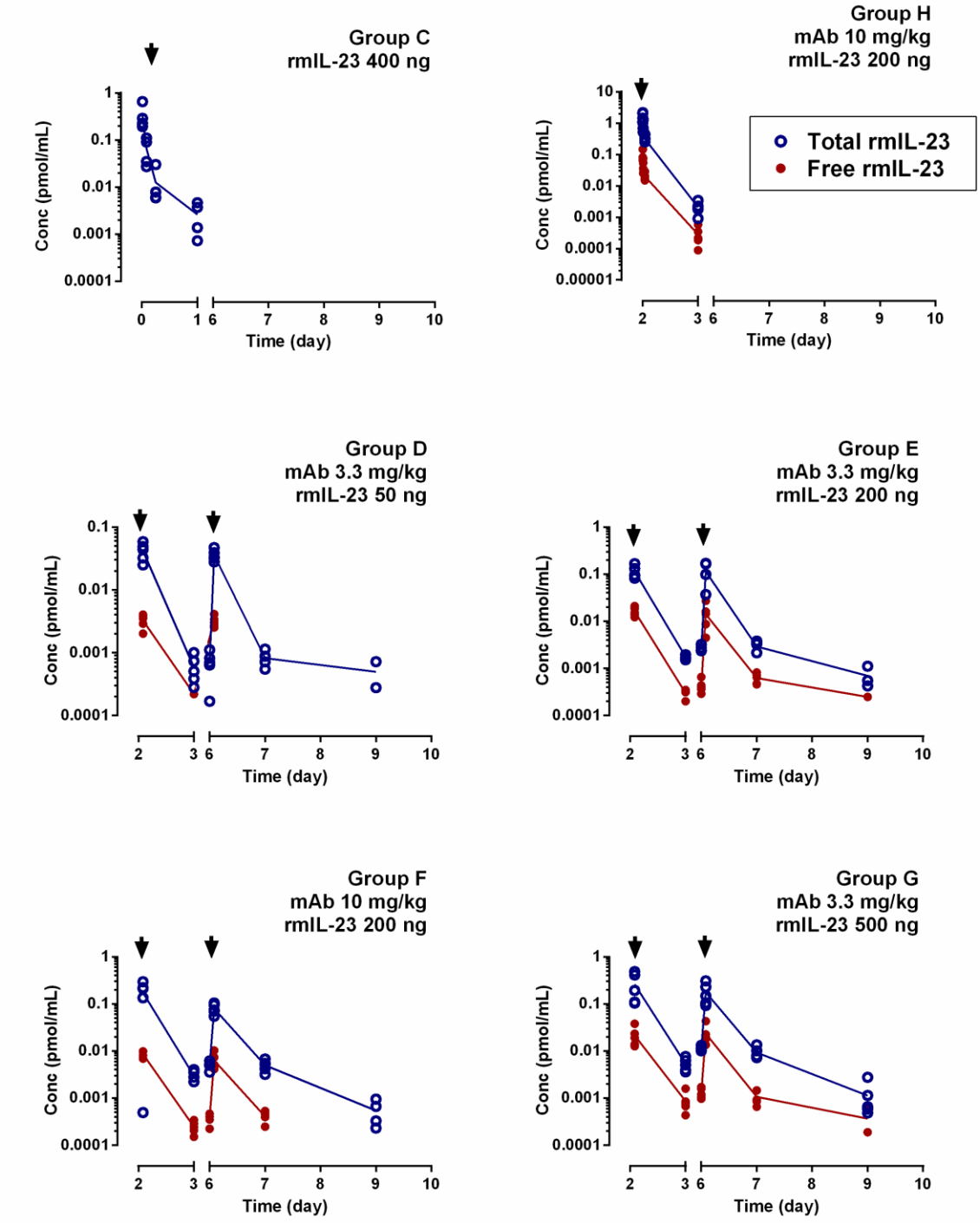

JPET Fast Forward. Published on February 2, 2018 as DOI: 10.1124/jpet.117.244855
This article has not been copyedited and formatted. The final version may differ from this version.

Figure 7

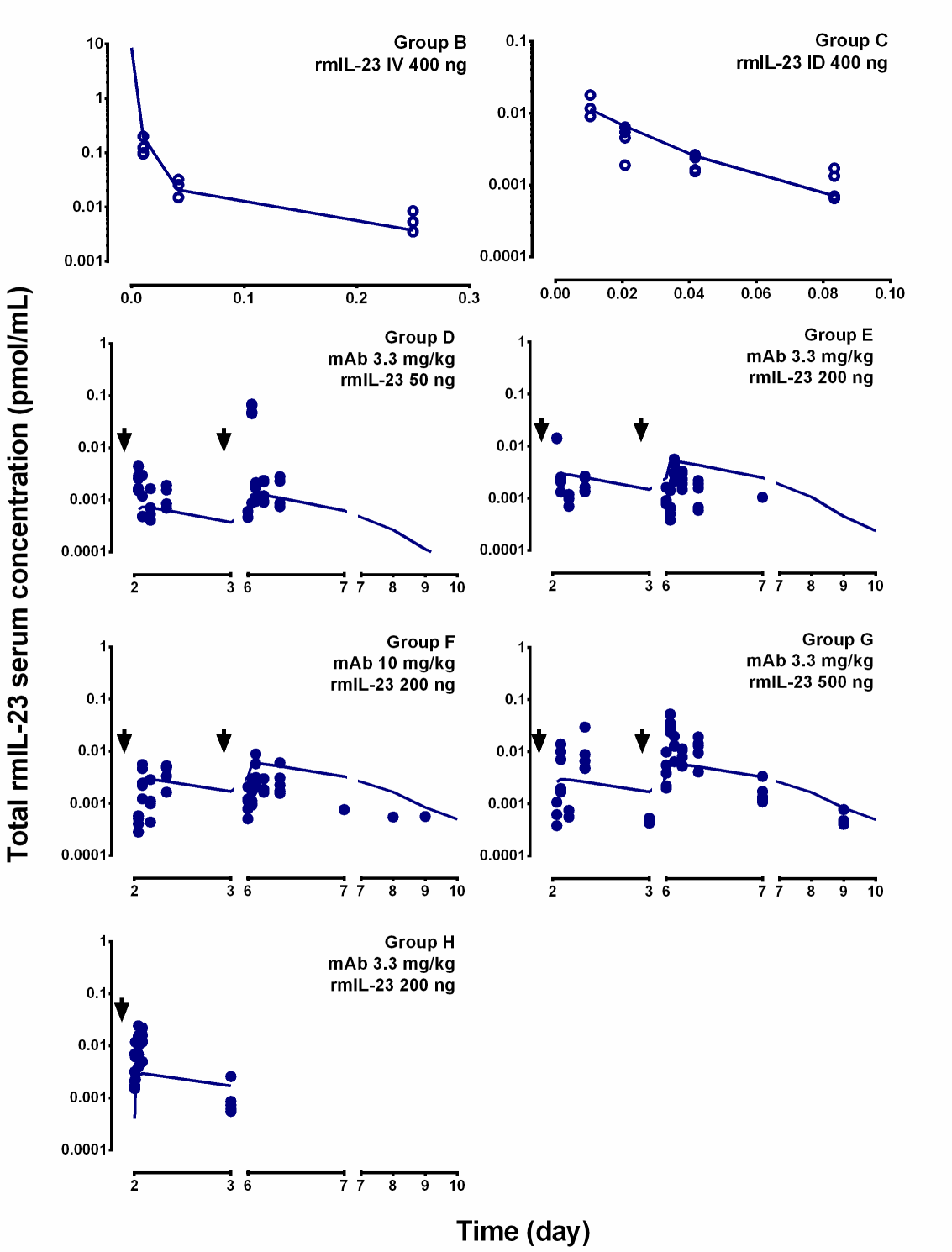

JPET Fast Forward. Published on February 2, 2018 as DOI: 10.1124/jpet.117.244855
This article has not been copyedited and formatted. The final version may differ from this version.

Figure 8

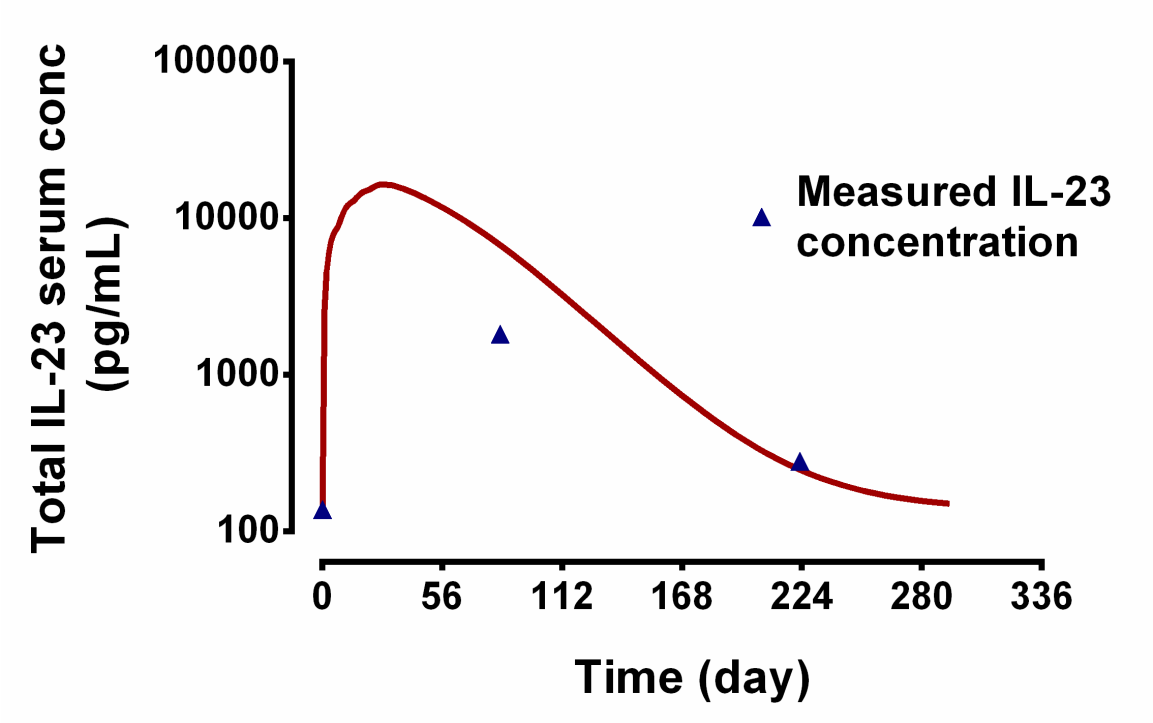

JPET Fast Forward. Published on February 2, 2018 as DOI: 10.1124/jpet.117.244855
This article has not been copyedited and formatted. The final version may differ from this version.

Figure 9